Journal of Power Sources 191 (2009) 233–239

Contents lists available at ScienceDirect

Journal of Power Sources

journal homepage: www.elsevier.com/locate/jpowsour

Influence of reaction temperature on the particle-composition distributions and activities of polyol-synthesized Pt-Ru/C catalysts for methanol oxidation

Lin Gan[a,b], Hongda Du[b], Baohua Li[b], Feiyu Kang[a,*]

[a] Laboratory of Advanced Materials, Department of Materials Science and Engineering, Tsinghua University, Beijing 100084, China
[b] Institute of Advanced Materials, Graduate School at Shenzhen, Tsinghua University, Shenzhen 518055, China

ARTICLE INFO

Article history:
Received 7 January 2009
Received in revised form 13 February 2009
Accepted 16 February 2009
Available online 3 March 2009

Keywords:
Polyol synthesis
Pt-Ru catalysts
Particle-composition distribution
Ruthenium oxide
Direct methanol fuel cells

ABSTRACT

We synthesized three kinds of Pt-Ru/C catalysts (denoted as a, b, and c) through conventional polyol process by heating the reaction solutions to different temperatures (120, 160 and 180 °C, respectively) and the fourth kind of catalyst (denoted as d) through a modified polyol process at 180 °C. By using scanning transmission electron microscopy combined with energy dispersive X-ray line analysis, we found that a higher reaction temperature resulted in more uniform particle-compositions of the Pt-Ru catalysts, which could be ascribed to the influence of temperature on the reduction rates of metal ions. The Pt-Ru/C-a catalyst showed a bimodal particle-composition distribution, while the Pt-Ru/C-d catalyst showed the narrowest unimodal distribution due to the highest temperature throughout the reaction. X-ray diffraction showed that all the Pt-Ru/C catalysts exhibited low alloying degrees of Ru with Pt. From high resolution transmission electron microscopy, we confirmed that the un-alloyed Ru was present in an amorphous form (likely RuO_x), and moreover, its distribution varied greatly in different catalysts. In the Pt-Ru/C-d catalyst, the amorphous RuO_x intimately contacted with the Pt/Pt-rich alloy, forming nanocomposite particles. The most uniform compositions of Pt-Ru particles in the Pt-Ru/C-d catalyst resulted in the highest electrocatalytic activity on methanol oxidation.

1. Introduction

Polyol synthesis has been widely adopted to prepare carbon supported Pt-Ru nanoparticles [1–8], which are used as the electrocatalysts for the anode methanol oxidation in direct methanol fuel cells. In a typical polyol process, ethylene glycol (EG) solution of mixed metal precursors (e.g. H_2PtCl_6 and $RuCl_3$) was heated to an elevated temperature to reduce the metal ions, where EG acted as both solvent and reducing agent. The formed metal particles were then subsequently or in-situ deposited on a suitable carbon support (e.g. carbon black). Previous works on the polyol synthesis are mainly focused on the size control of metal nanoparticles by tailoring the pH value of the reaction solutions [1,9,10]. However, on the basis of the well-known bi-functional mechanism [1], it is noted that the electrocatalytic activity of Pt-Ru catalysts on the methanol oxidation is not only dependent on their sizes, but also strongly dependent on the distribution of Pt and Ru sites at the atomic level. And, it is generally considered that the 50:50 at% Pt-Ru alloy is the most beneficial in this regard [1,11]. Nevertheless, Rolison and coworkers [12] argued that the un-alloyed structure consisted of Pt metal and amorphous hydrous ruthenium oxide ($RuO_2{\cdot}xH_2O$) was more active than the alloyed one due to the high electron and proton conductivity. This point was also demonstrated recently by Cao et al. [13], who further proposed that the $RuO_2{\cdot}xH_2O$ could donate hydroxide species more easily to Pt sites to aid CO oxidation than the alloyed Ru.

In most works on the polyol-synthesized Pt-Ru catalysts [1,2,14,15], it was reported that Ru was only partially dissolved in the face-centered cubic Pt lattice (i.e. formed alloy with Pt) and a separate amorphous oxidized Ru species (RuO_x) might also existed [1,15]. In the reference [2], it was even reported that the Pt-Ru particles did not form alloy. Guo et al. [15] further suggested that the active material of Ru in the polyol-synthesized Pt-Ru/C catalysts was un-alloyed amorphous RuO_x instead of alloyed Ru. Whether the promotion effect comes from the alloyed Ru with Pt or comes from the $RuO_2{\cdot}xH_2O/RuO_x$, it is believed that an intimate contact of a certain amount of Ru species with Pt in each individual particle, i.e. a uniform composition of Pt-Ru particles, is crucial to maximize the promotion effect of Ru for high catalytic activity. However, there are few reports on the control of a uniform composition of Pt-Ru particles during the polyol synthesis, and how the amorphous Ru species distributed in the polyol-synthesized catalysts is still unknown up to now. Central to this work is therefore to explore such question. On the other hand, the influences of solution pH value [1,16] and

* Corresponding author. Tel.: +86 10 62792618; fax: +86 10 62792911.
E-mail address: fykang@tsinghua.edu.cn (F. Kang).

0378-7753/$ – see front matter © 2009 Elsevier B.V. All rights reserved.
doi:10.1016/j.jpowsour.2009.02.042

reaction atmosphere [14] during the polyol synthesis on the characteristics and activities of the Pt-Ru/C catalysts have been explored. However, there are few studies on the influence of the reaction temperature, although a wide range of temperatures (110–198 °C) [1–3,11,15,16] has been adopted during the polyol synthesis. In this work, we find that the reaction temperature has a great influence on the particle-composition distributions and therefore the activities of polyol-synthesized Pt-Ru/C catalysts. The structure and the distribution of the Ru species and their influence on the catalytic activities towards methanol oxidation were investigated.

2. Experimental

$H_2PtCl_6{\cdot}6H_2O$ and $RuCl_3{\cdot}xH_2O$ were used as the precursors of Pt-Ru catalysts, and Vulcan XC carbon black was used as catalyst support. The Pt-Ru/C (20 wt.% Pt and 10 wt.% Ru) catalysts were synthesized through a conventional polyol process [3,5,15] and a modified polyol process, where the temperatures were controlled differently. For comparison, Pt/C (20 wt.% Pt) catalyst was also synthesized through the modified polyol process.

(1) In the conventional polyol process, 140 mg carbon support, 860 μL mixed EG solution of H_2PtCl_6 and $RuCl_3$ (containing 40 mg Pt and 20 mg Ru), and 1.42 mL EG solution of NaOH (1.0 mol L^{-1}) were added to 50 mL EG with magnetic stirring and ultrasonic treatment to form a homogeneous solution. The pH value of the reaction solution was ca. 10.0. The whole solution was then heated from room temperature to 120, 160, or 180 °C within ca. 15 min by being placed in a pre-heated oil bath. After 3 h reaction, the solution was cooled and then filtered. The obtained catalyst was denoted as Pt-Ru/C-a, Pt-Ru/C-b and Pt-Ru/C-c, respectively.

(2) In the modified polyol process, 140 mg carbon support and 1.42 mL EG solution of NaOH (1.0 mol L^{-1}) were added to 50 mL EG with magnetic stirring and ultrasonic treatment to form a homogeneous solution. The solution was then heated to 180 °C in an oil bath. When the solution reached 180 °C, 860 μL mixed EG solution of H_2PtCl_6 and $RuCl_3$ (containing 40 mg Pt and 20 mg Ru) were quickly added. After 10 min reaction, the whole solution was cooled and then filtered. The obtained catalyst was denoted as Pt-Ru/C-d. The process for preparing Pt/C catalyst is similar, except that the relative amount of H_2PtCl_6 and NaOH was adjusted. For all the catalysts synthesized above, the weight calculation indicated that the Pt or Pt-Ru conversion was nearly 100% during the reduction and deposition on carbon support.

Transmission electron microscopy (TEM) and high resolution TEM (HRTEM) were performed on JEOL-2100F operated at 200 kV. Angular dark field (ADF) images were taken in scanning TEM (STEM) mode with an energy dispersive X-ray (EDX) spectrometer. A slightly larger probe size of 0.7 nm was used to generate a higher X-ray signal, and an automatic specimen-drift correction technique was used. Powdered X-ray diffraction (XRD) was performed with a filtered Cu-Kα radiation. The 2θ angular range between 15° and 90° was explored at a scanning rate of 4° min^{-1} in the resolution of 0.017°. Silicon powder was homogeneously grounded with the catalyst sample to be used as an internal standard.

The electrochemical measurements were performed in single compartment with three-electrode cell at room temperature. To prepare the working electrode, 10.0 mg of the catalyst sample was

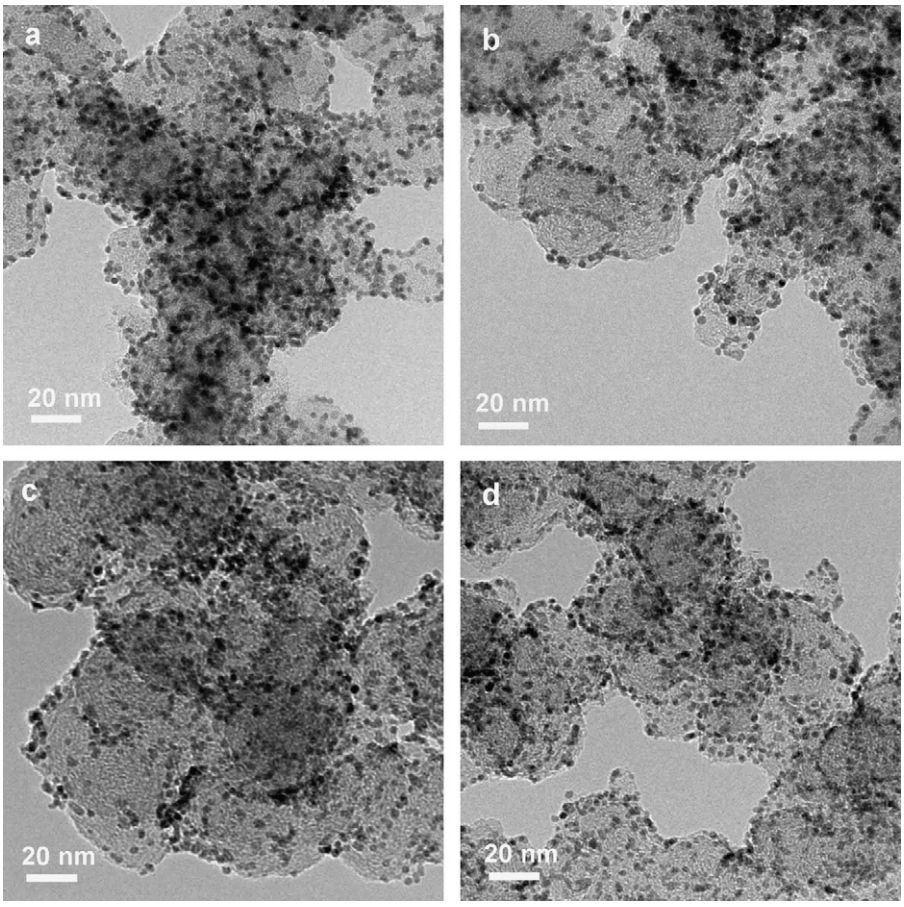

Fig. 1. TEM images of the Pt-Ru/C catalysts. (a) Pt-Ru/C-a, (b) Pt-Ru/C-b, (c) Pt-Ru/C-c, and (d) Pt-Ru/C-d.

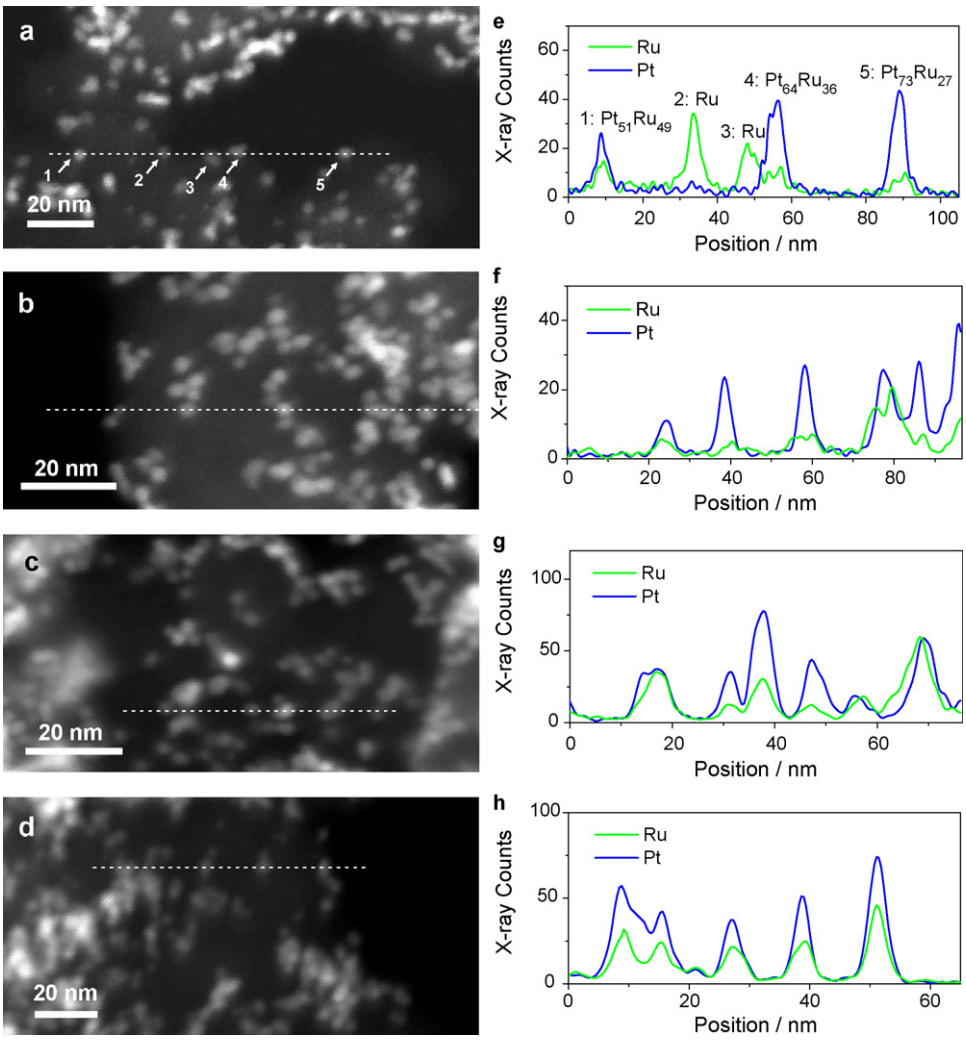

Fig. 2. STEM-ADF images (a, b, c and d) and EDX line analysis (e, f, g and h) along the dash lines indicated in (a, b, c and d) for the Pt-Ru/C-a, Pt-Ru/C-b, Pt-Ru/C-c and Pt-Ru/C-d catalyst, respectively. As a guide, the compositions of Pt-Ru particles along the dash line in (a) were determined from the areas of the peaks in (e).

dispersed in 900 μL isopropanol +100 μL Nafion solution (5 wt.%, DuPont), and then ultrasonically dispersed for 15 min to form a uniform suspension. Then 1.0 μL of the suspension was dropped onto a glassy carbon electrode (3.0 mm in diameter) to form a uniform catalyst layer that was then dried at 60 °C for 15 min. A Pt foil was used as the counter electrode and a Hg/Hg_2SO_4 electrode was used as the reference electrode. All the potentials referred in this paper are with respect to normal hydrogen electrode (NHE).

3. Results and discussion

Fig. 1a–d shows the TEM images of the synthesized Pt-Ru/C-a, Pt-Ru/C-b, Pt-Ru/C-c and Pt-Ru/C-d catalyst, respectively. As shown in Fig. 1, the Pt-Ru nanoparticles are well dispersed on the carbon supports and exhibit similar particle sizes in the range of 2–3 nm in all the Pt-Ru/C catalysts. Therefore, the reaction temperature seems to have no significant influence on the particle sizes of Pt-Ru catalysts. In a number of references [1,9,10], it was reported that the pH value of the reaction solution played an important role in the size control of metal nanoparticles. In this study, all the Pt-Ru/C catalysts were prepared using the same amount of alkali (i.e. the same pH value) and therefore showed similar particle sizes of Pt-Ru.

From the large area EDX analysis in TEM, all the Pt-Ru/C catalysts were confirmed to possess the same composition of Pt-Ru as the nominal atomic ratio, i.e. Pt:Ru = 1:1. To study the composition distribution of the Pt-Ru particles at nanoscale, we further performed STEM coupled with EDX line analysis. Fig. 2a shows the STEM image of the Pt-Ru/C-a catalyst. An EDX line spectrum was acquired along the white line marked in Fig. 2a, and the Pt and Ru counts were plotted over the scanning distance, as shown in Fig. 2e. By measuring the areas of the peaks in Fig. 2e and using the Cliff–Lorimer equation [17,18], we could determine the atomic ratio of Pt:Ru for each Pt-Ru particle. In the Pt-Ru/C-a catalyst, we found that the distributions of Pt and Ru showed significant segregation: some particles exhibited Pt-rich compositions (e.g. particle 4 and 5); while some particles showed Ru-rich compositions or even consisted of only Ru (e.g. particle 2 and 3). In the Pt-Ru/C-b catalyst (Fig. 2b), the compositions of Pt-Ru particles became more uniform, and no particles that consisted of only Ru were found, as shown in Fig. 2f. However, there is still some fluctuation of the atomic concentration of Ru. Such fluctuation also exists in the Pt-Ru/C-c catalysts (Fig. 2 c and g). However, in the Pt-Ru/C-d catalyst shown in Fig. 2d, we find that the atomic concentration of Ru becomes quite uniform and shows little fluctuation along the scanned Pt-Ru particles (Fig. 2 h).

To gain a certain extent of statistical meaning, we performed similar STEM-EDX line analysis over 40–50 particles in each kind of Pt-Ru/C catalysts. The histograms of the particle-composition distributions of Pt-Ru in different Pt-Ru/C catalysts are plotted in Fig. 3. In the Pt-Ru/C-a catalyst synthesized at 120 °C, the compositions of Pt-Ru particles exhibit a bimodal distribution, i.e. Pt-rich parti-

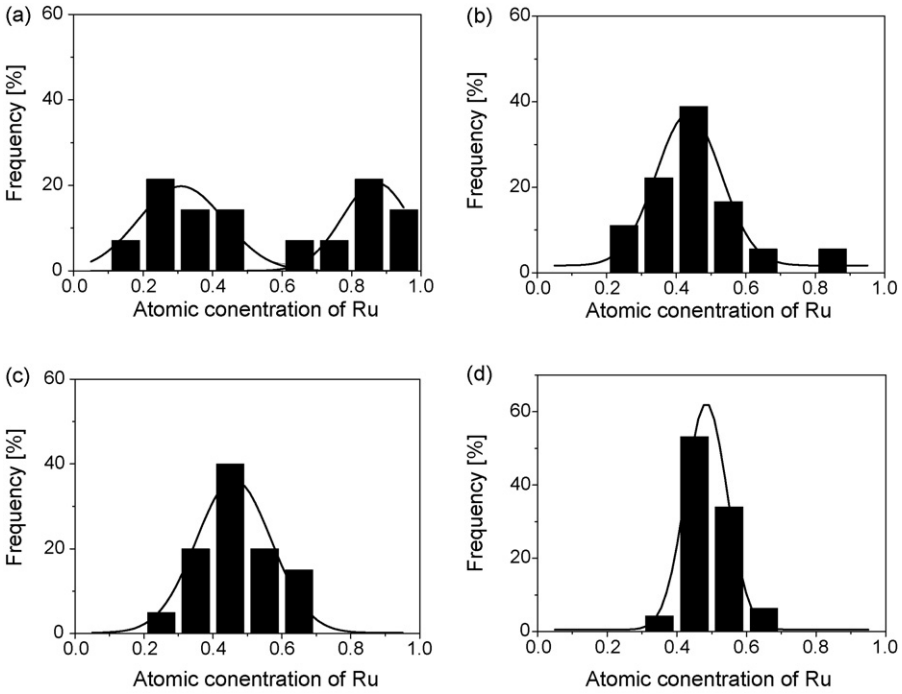

Fig. 3. Histograms of composition distributions of Pt-Ru particles in (a) Pt-Ru/C-a, (b) Pt-Ru/C-b, (c) Pt-Ru/C-c and (d) Pt-Ru/C-d catalyst.

cles and Ru-rich particles, suggesting significant segregation. In the Pt-Ru/C-b catalyst synthesized at 160 °C, the compositions of Pt-Ru particles become to show a unimodal distribution, as shown in Fig. 3b. However, the distribution appears quite wide. A likewise wide composition distribution is shown in the Pt-Ru/C-c catalyst synthesized at 180 °C (Fig. 3c), indicating that further increase of temperature in the conventional polyol process did not produce more uniform compositions. However, it is exciting that the compositions of Pt-Ru particles show quite a narrow distribution in the Pt-Ru/C-d catalyst synthesized by the modified polyol process at 180 °C, as shown in Fig. 3d.

The STEM-EDX analysis therefore shows a great influence of reaction temperature on the particle-composition distributions of the polyol-synthesized Pt-Ru catalysts. A higher reaction temperature would generally result in more uniform compositions with a narrower distribution. This result may be possibly originated from the different reduction kinetics of the two types of precursors (i.e. $PtCl_6^{2-}$ and Ru^{3+}). Previous studies on the polyol synthesis of Pt-Ru catalysts showed that some Ru^{3+} ions failed to be reduced simultaneously with $PtCl_6^{2-}$, which might be due to the lower redox potential of Ru^{3+}/Ru ($E^\circ \sim 0.62$ V) compared with $PtCl_6^{2-}$/Pt ($E^\circ \sim 0.74$ V) [3,15,19]. It should be noted here that the detailed reduction mechanism might be much more complicated because hydrolysis of metal ions might occur and metal hydroxide could form especially at alkaline conditions [16]. Although the detailed mechanism was unclear, Lee et al. [11] found that the reduction path of Ru^{3+} was very complex compared with that of $PtCl_6^{2-}$ by using UV–vis spectrum. We therefore speculate that, the reduction of Ru^{3+} might be more difficult and thus showed larger apparent activation energy than that of $PtCl_6^{2-}$ during the polyol synthesis. Therefore, at a low reaction temperature, $PtCl_6^{2-}$ might be reduced faster than Ru^{3+} and thus Pt-rich particles would form at the early stage of the reaction. When $PtCl_6^{2-}$ were over-consumed during the course of the reduction, the concentration of Ru^{3+} became larger than that of $PtCl_6^{2-}$ and thus Ru-rich particles would form at the later stage. This situation coincides very well with the bimodal composition distribution shown in the Pt-Ru/C-a catalyst. When the reaction temperature increased, it is noted that the rate of the reaction with higher activation energy would increase more significantly than that of the reaction with lower activation energy, according to the well-known Arrhenius relationship. Therefore, the Ru^{3+} reduction would be accelerated more significantly than the $PtCl_6^{2-}$ reduction, and thus the difference of the reduction rates between the two types of metal ions could be minished. In another word, a higher reaction temperature could activate the simultaneous reduction of Ru^{3+} with $PtCl_6^{2-}$ and lead to more uniform compositions. This is clearly demonstrated in the Pt-Ru/C-b catalyst (Fig. 3b) compared with the Pt-Ru/C-a catalyst.

From Fig. 3c, one can see that the Pt-Ru/C-c catalyst shows no more uniform compositions compared with the Pt-Ru/C-b catalyst, though the former was synthesized at a higher temperature. This result could be ascribed to a limit control of the real reaction temperature in the conventional polyol process. Bock et al. found that,

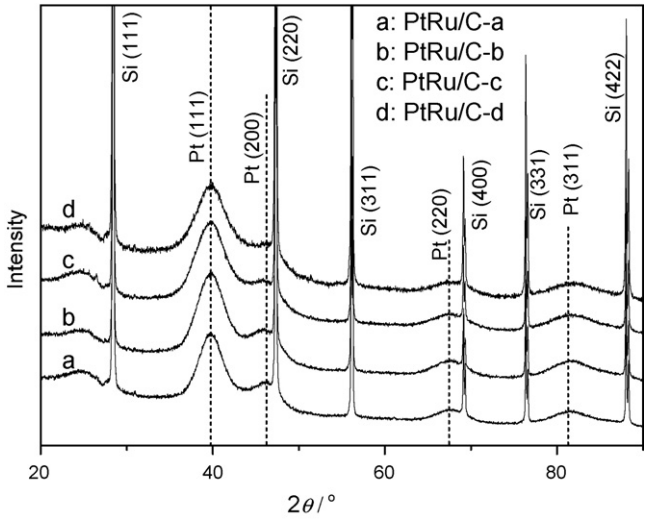

Fig. 4. XRD patterns of the Pt-Ru/C catalysts. Silicon powder was homogeneously added as an internal standard. Column plot in dash lines is PDF#040802 for Pt.

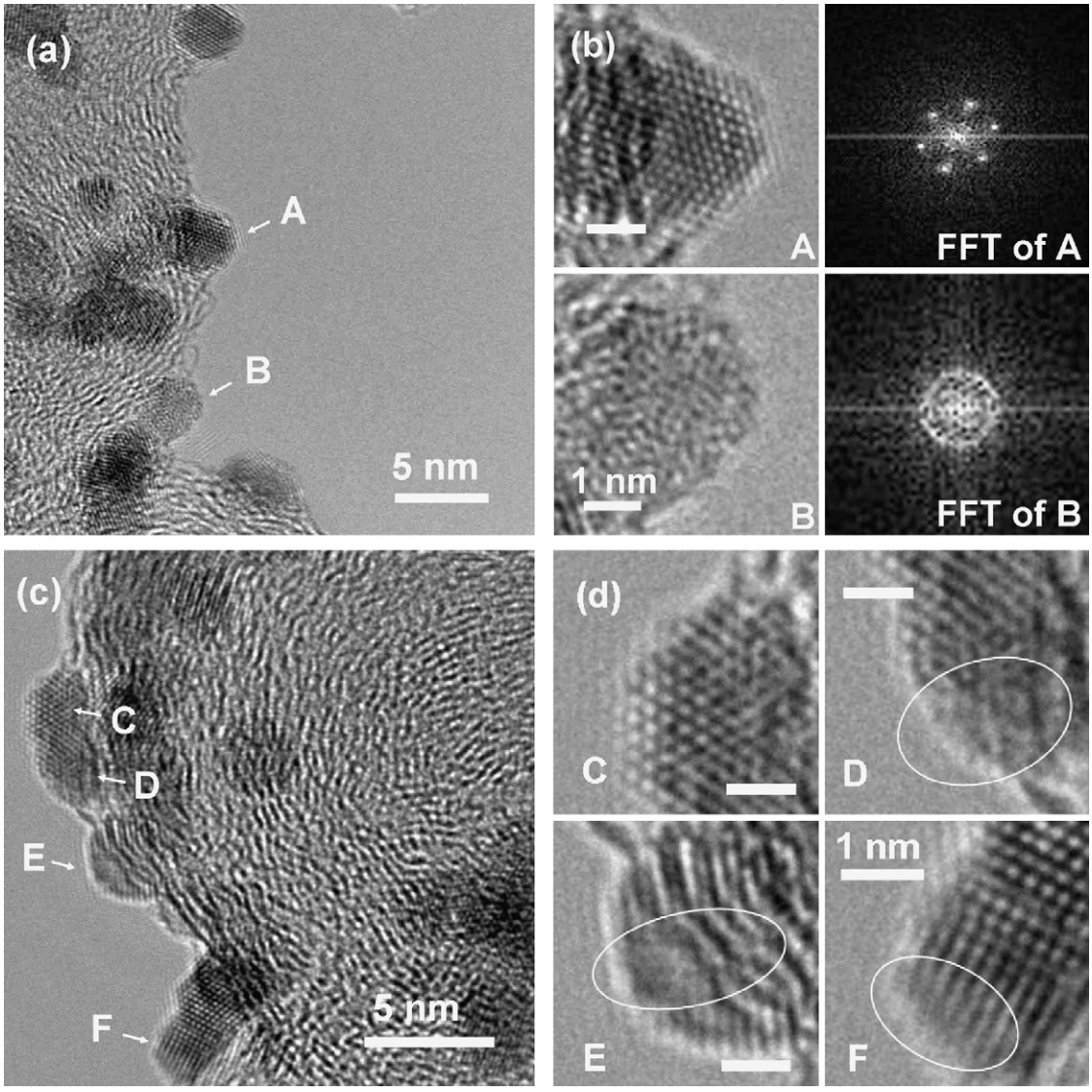

Fig. 5. HRTEM images of (a and b) Pt-Ru/C-a, and (c and d) Pt-Ru/C-d catalyst. The enlarged images of particle 'A' and 'B' in (a) and their corresponding FFT patterns are shown in (b). The enlarged images of particle 'C', 'D', 'E' and 'F' in (c) are shown in (d), where the circles indicate the amorphous part of the particles. All the scale bars in (b) and (d) represent 1 nm.

though the reaction solution was heated from room temperature to 160 °C within 20 min, the reduction of Pt-Ru would complete within 5 min and the solution temperature reached ca. 130 °C within this time [1]. Therefore, despite the Pt-Ru/C-b and Pt-Ru/C-c catalyst were synthesized under the nominal temperature of 160 and 180 °C, respectively, the actual reaction temperatures may be similarly lower ones, leading to both wide composition distributions. Based on this result, we believed that, once a higher actual reaction temperature was achieved, the compositions of Pt-Ru particles would be more uniform. This point is well illustrated in the Pt-Ru/C-d catalyst synthesized through the modified polyol process, where the actual reaction temperature could be steadily controlled at 180 °C throughout the synthesis. The Pt-Ru/C-d catalyst shows the most uniform compositions with the narrowest distribution, as clearly shown in Fig. 3d.

To explore the crystalline structure of the Pt-Ru particles, we carried out XRD measurements. The XRD data shown in Fig. 4 were collected with Si as an internal standard. The diffraction peaks of the face-centered cubic Pt lattice are clearly recognized in all the catalysts. As reported in other references [1,5,15], we found no diffraction peaks for Ru, which could be ascribed to a number of reasons such as forming Pt-Ru alloy or the Ru being present in the amorphous form. By fitting the Pt (2 2 0) peaks after background subtracting, we found that the positions of the Pt (2 2 0) peaks for the four kinds of catalysts were all quite close to that for pure Pt. The lattice parameter estimated from Pt (2 2 0) peak for the Pt-Ru/C-d catalyst is 0.3905 nm, which is slightly smaller than the reported value for pure Pt (0.3916 nm). Calculating by the formula reported by Antolini and Cardellini [20], we found that only a small amount of Ru formed alloy with Pt (ca. 8 at% Ru in alloyed Pt-Ru). Similar results were obtained from the other catalysts, while accurate values of alloying extent are not listed here due to calculated errors from the broad Pt (2 2 0) peaks. The XRD results therefore indicate that most of Ru did not form alloy with Pt and they might be amorphous [1,15]. By using temperature-programmed reduction, Guo et al. [15] found that the un-alloyed amorphous Ru were generally in a form of oxidized state, i.e. RuO_x. Li et al. [14] further reported that the high content of oxidized Ru species in the un-alloyed Pt-Ru catalysts was attributed to re-oxidation of Ru colloids by oxygen in air during the catalyst preparation. Whether the RuO_x contained structural water (i.e. formed hydrous RuO_x) or not is still unclear now and needs further studies.

The amorphous Ru species were clearly identified by HRTEM images, and moreover, their distribution seemed to be quite different in different catalysts. In the Pt-Ru/C-a catalyst shown in Fig. 5a, two distinct structure of the supported particles could be found, i.e. particle 'A' that seems to be crystalline and particle 'B' that shows to be amorphous, as confirmed by the corresponding fast Fourier transformed (FFT) patterns shown in Fig. 5b. The amorphous particle 'B' could be therefore identified as an individual RuO_x particle, which is also in agreement with the STEM-EDX analysis result shown in Fig. 2b. In contrary, individual amorphous particles were rarely observed in the Pt-Ru/C-d catalyst, as shown in Fig. 5c. Interestingly, we found that a number of particles, e.g. particle 'D', 'E' and 'F', showed a composite structure. A careful examination of their enlarged images in Fig. 5d indicates that these particles generally consist of an amorphous part that intimately contacts with a crystalline part, which may correspond to the RuO_x species and Pt/Pt-rich alloy, respectively. Since the HRTEM images only generate two-dimensional information by projecting from a three-dimensional structure [21] and the amorphous phase shows much lower contrast compared with the crystalline phase, we could not determine the actual three-dimensional distribution of the amorphous RuO_x species in the composite particles. Similarly, one could not identify the particle 'A' and 'C' to be completely crystalline ones. However, a comprehensive analysis of the HRTEM images with the STEM-EDX and XRD results could show us that, the distribution of the amorphous RuO_x varied greatly in the catalysts, i.e. the higher the reaction temperature, the more uniform the distribution of amorphous RuO_x in the Pt-Ru particles.

To study the electrocatalytic activities of the catalysts, we also synthesized Pt/C catalyst by the modified polyol process for comparison. TEM images (not shown here) confirmed that the Pt/C catalyst also showed a good dispersion of the Pt particles with the sizes in the range of 2–3 nm. We then characterized all the catalysts by cyclic voltammetry in nitrogen saturated 0.1 mol L^{-1} $HClO_4$ aqueous solution, as shown in Fig. 6. The voltammograms clearly show the hydrogen adsorption/desorption in the potential region of ca. 0–0.3 V. The Pt electroactive surface area (ESA) could be estimated from the integrate charge associated with the hydrogen adsorption [22]. The values are 65, 43, 54, 56 and 56 m^2/g for Pt/C, Pt-Ru/C-a, Pt-Ru/C-b, Pt-Ru/C-c and Pt-Ru/C-d catalyst, respectively. It can be seen that all the Pt-Ru/C catalysts show lower ESA values than the Pt/C catalyst, possibly because the addition of Ru caused the Pt surface sites partially covered [22]. In addition, the Pt-Ru/C-a catalyst also shows lower ESA than the other Pt-Ru/C catalysts. The reason for this is unclear, but possibly could be that, the deposition of Ru was much slower than that of Pt in the Pt-Ru/C-a catalyst, and therefore Ru might deposit on pre-formed Pt nuclei and formed Pt-core/Ru-shell particles, which resulted in less Pt surface sites.

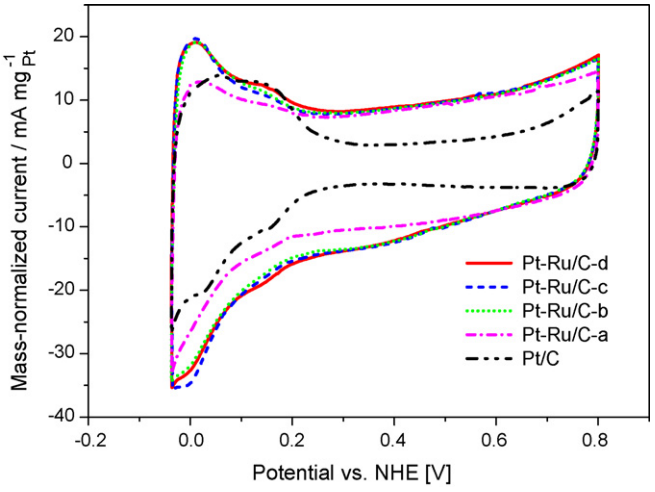

Fig. 6. Cyclic voltammograms on different catalyst electrodes in N_2 saturated 0.1 mol L^{-1} $HClO_4$ aqueous solution at a scanning rate of 20 mV s^{-1}. All the curves refer to the voltammograms in the 20th cycle, where a steady response was obtained. The currents were normalized to the mass of Pt.

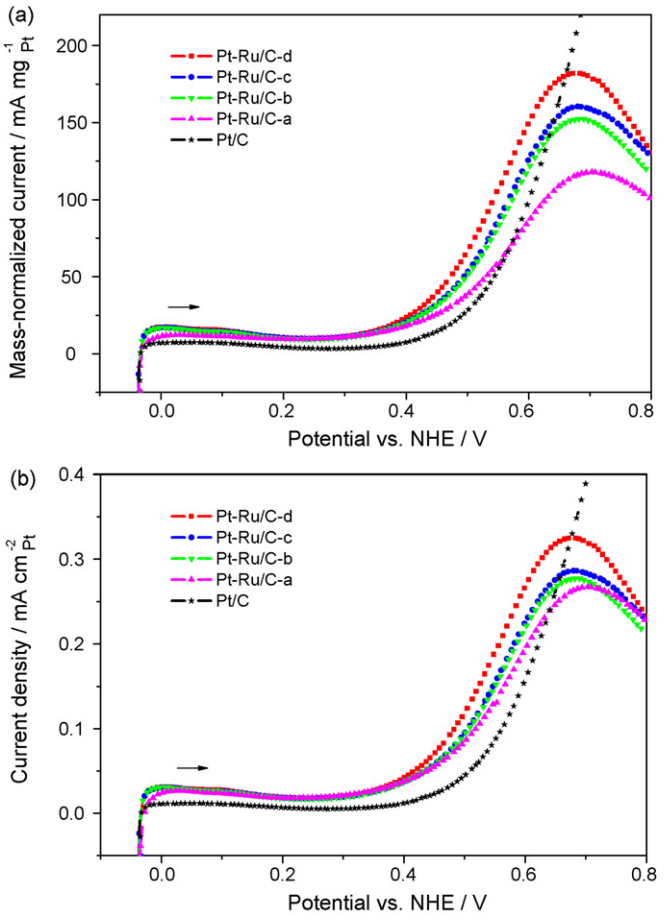

Fig. 7. Voltammograms of methanol oxidation on different catalyst electrodes in N_2 saturated 1.0 mol L^{-1} CH_3OH + 0.1 mol L^{-1} $HClO_4$ aqueous solution at a scanning rate of 20 mV s^{-1}. The currents are normalized to (a) the mass and (b) the ESA of Pt. For clarity, all the curves refer to the forward part of the cyclic voltammograms in the 20th cycle, where a steady response was obtained.

We further performed cyclic voltammetry measurements of all the catalysts in nitrogen saturated 1.0 mol L^{-1} CH_3OH +0.1 mol L^{-1} $HClO_4$ aqueous solution to investigate their electrocatalytic activities towards methanol oxidation. Fig. 7a shows the voltammograms in terms of mass-normalized currents that represent the overall catalytic activities. In the potential region of 0.4–0.5 V relevant to fuel cell research, the mass-normalized currents are in the order of Pt-Ru/C-d > Pt-Ru/C-c ≈ Pt-Ru/C-b > Pt-Ru/C-a > Pt/C. To reveal the effect of intrinsic catalytic activities, Fig. 7b shows the currents normalized to the ESA of all the catalysts. It can be seen that the intrinsic catalytic activities in the potential region of 0.4–0.5 V are also in the order of Pt-Ru/C-d > Pt-Ru/C-c ≈ Pt-Ru/C-b > Pt-Ru/C-a > Pt/C. We further measured the steady-state chronoamperometric curves at a given potential of 0.5 V. As shown in Fig. 8, the steady-state current density on the Pt-Ru/C-d catalyst (0.116 mA $cm^{-2}{}_{Pt}$) is enhanced to ca. 150% of that on Pt-Ru/C-b and Pt-Ru/C-c (0.078 mA $cm^{-2}{}_{Pt}$), 180% of that on Pt-Ru/C-a (0.065 mA $cm^{-2}{}_{Pt}$), and 720% of that on Pt/C (0.016 mA $cm^{-2}{}_{Pt}$). The enhancement in the intrinsic catalytic activities of Pt-Ru/C catalysts compared with Pt/C catalyst is significant, which clearly demonstrates the promotion effect of Ru. Moreover, when we correlate the order of catalytic activities with the structure characterization results, it can be concluded that, the more

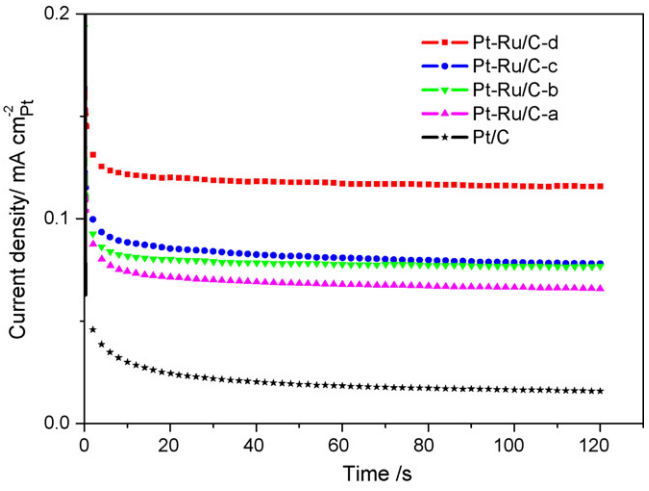

Fig. 8. Chronoamperometric curves of methanol oxidation on different catalyst electrodes at 0.5 V in N_2 saturated 1.0 mol L^{-1} CH_3OH + 0.1 mol L^{-1} $HClO_4$ aqueous solution. The currents are normalized to the ESA of Pt.

uniform the particle-compositions, the higher the catalytic activities of Pt-Ru/C catalysts. The highest intrinsic catalytic activity of the Pt-Ru/C-d catalyst is therefore definitely ascribed to the most uniform particle-compositions, which could maximize the utilization and thus the promotion effect of Ru. It should be noted that, besides the particle-composition, the chemical state of Ru in the Pt-Ru particles may also have an important influence on the catalytic activities. The composite Pt-RuO_x structure, i.e. amorphous RuO_x on Pt, was shown in this work. However, the detailed benefits of the composite Pt-RuO_x, especially its superiority over alloyed Pt-Ru in the electrocatalysis of methanol oxidation, are not within the scope of this work. In fact, this point is still controversial and conflicted results seem to be shown in different references [12,14]. Therefore, further detailed studies are needed regarding on this issue.

Our work also demonstrates that a high reaction temperature throughout the polyol synthesis is necessary to achieve a uniform particle-composition of Pt-Ru/C catalysts, and this condition could be easily realized in the modified polyol process. This result may also be helpful to understand possible advantages of the recently developed microwave-polyol process for the synthesis of Pt-Ru/C catalysts [7,22], where the reaction solution could be rapidly heated (normally, within 1–2 min) to a high temperature (e.g. the boiling point of EG, 198 °C) under the microwave irradiation. Such rapid heating may be beneficial to achieve a high reaction temperature throughout the synthesis and therefore results in a uniform particle-composition of the Pt-Ru/C catalysts.

4. Conclusion

During the polyol synthesis of Pt-Ru/C catalysts, the reaction temperature has a great influence on the composition distributions of the Pt-Ru particles, which could be ascribed to the influence on the different reduction rates of the two types of metal precursors. A higher reaction temperature would promote the simultaneous reduction of Pt and Ru precursors, thus leading to more uniform compositions of Pt-Ru particles. All the Pt-Ru/C catalysts showed quite a low alloying degree of Pt-Ru and contained amorphous RuO_x, while the distribution of RuO_x were quite different. The Pt-Ru/C-a catalyst synthesized at the lowest temperature showed a bimodal particle-composition distribution and contained individual RuO_x particles. In contrary, due to the highest reaction temperature throughout the synthesis, the Pt-Ru/C-d catalyst showed the most uniform compositions of Pt-Ru particles, in which the amorphous RuO_x intimately contacted with the Pt/Pt-rich alloy. The Pt-Ru/C-d catalyst with the most uniform particle-compositions of Pt-Ru resulted in the highest electrocatalytic activity on methanol oxidation.

Acknowledgements

We thank the financial support from National Nature Science Foundation of China under Grant No. 50632040. We also appreciate SAE Magnetics Ltd. for their support on TEM measurement.

References

[1] C. Bock, C. Paquet, M. Couillard, G.A. Botton, B.R. MacDougall, J. Am. Chem. Soc. 126 (2004) 8028–8037.
[2] W.Z. Li, X. Wang, Z.W. Chen, M. Waje, Y.S. Yan, J. Phys. Chem. B 110 (2006) 15353–15358.
[3] J.S. Guo, G.Q. Sun, Q. Wang, G.X. Wang, Z.H. Zhou, S.H. Tang, L.H. Jiang, B. Zhou, Q. Xin, Carbon 44 (2006) 152–157.
[4] Y.M. Liang, H.M. Zhang, B.L. Yi, Z.H. Zhang, Z.C. Tan, Carbon 2005 (2005) 3144–3152.
[5] S.Y. Yan, G.Q. Sun, J. Tian, L.H. Jiang, J. Qi, Q. Xin, Electrochim. Acta 52 (2006) 1692–1696.
[6] H.D. Du, B.H. Li, L. Gan, P. Wu, F.Y. Kang, Y.Q. Zeng, New Carbon Mater. 23 (2008) 58–62.
[7] M. Tsuji, M. Kubokawa, R. Yano, N. Miyamae, T. Tsuji, M.S. Jun, S. Hong, S. Lim, S.H. Yoon, I. Mochida, Langmuir 23 (2007) 387–390.
[8] K.T. Jeng, C.C. Chien, N.Y. Hsu, S.C. Yen, S.D. Chiou, S.H. Lin, W.M. Huang, J. Power Sources 160 (2006) 97–104.
[9] Y. Liang, D.W. Liao, Acta Phys. Chim. Sin. 24 (2008) 317–322.
[10] X. Li, W.X. Chen, J. Zhao, W. Xing, Z.D. Xu, Carbon 43 (2005) 2168–2174.
[11] D. Lee, S. Hwang, I. Lee, J. Power Sources 160 (2006) 155–160.
[12] J.W. Long, R.M. Stround, K.E. Swider-Lyons, D.R. Rolison, J. Phys. Chem. B 104 (2000) 9772–9776.
[13] L. Cao, F. Scheiba, C. Roth, F. Schweiger, C. Cremers, U. Stimming, H. Fuess, L.Q. Chen, W.T. Zhu, X.P. Qiu, Angew. Chem. Int. Ed. 45 (2006) 5315–5319.
[14] H.Q. Li, G.Q. Sun, Y. Gao, Q. Jiang, Z.Q. Jia, Q. Xin, J. Phys. Chem. C 111 (2007) 15192–15200.
[15] J.S. Guo, G.Q. Sun, S.G. Sun, S.Y. Yan, W.Q. Yang, J. Qi, Y.S. Yan, Q. Xin, J. Power Sources (2007) 299–306.
[16] L. Ren, Y.C. Xing, Electrochim. Acta 53 (2008) 5563–5568.
[17] P.A. Midgley, J.M. Thomas, L. Laffont, M. Weyland, R. Raja, B.F.G. Johnson, T. Khimyak, J. Phys. Chem. B 108 (2004) 4590–4592.
[18] J.Y. Liu, Microsc. Microanal. 10 (2004) 55–76.
[19] Z.L. Liu, X.Y. Ling, X.D. Su, J.Y. Lee, J. Phys. Chem. B 108 (2004) 8234–8240.
[20] E. Antolini, F. Cardellini, J. Alloys. Compd. 315 (2001) 118–122.
[21] M. Weyland, Top. Catal. 21 (2002) 175–183.
[22] Z.L. Liu, J.Y. Lee, Z.W. Chen, M. Han, L.M. Gan, Langmuir 20 (2004) 181–187.